Journal of Water Process Engineering 37 (2020) 101418

Contents lists available at ScienceDirect

Journal of Water Process Engineering

journal homepage: www.elsevier.com/locate/jwpe

Sonocatalytic degradation of rhodamine B using tin oxide/ montmorillonite

Is Fatimah[a,*], Rico Nurillahi[a], Imam Sahroni[a], Ganjar Fadillah[a], Bambang Hernawan Nugroho[b], Azlan Kamari[c], Oki Muraza[d]

[a] Department of Chemistry, Faculty of Mathematics and Natural Sciences, Universitas Islam Indonesia, Kampus Terpadu UII, Jl. Kaliurang Km 14, Sleman, Yogyakarta, Indonesia
[b] Nanopharmacy Research Center, Department of Pharmacy, Universitas Islam Indonesia, Kampus Terpadu UII, Jl. Kaliurang Km 14, Sleman, Yogyakarta, Indonesia
[c] Chemistry Department, Universiti Pendidikan Sultan Idris Perak, Perak 35900, Malaysia
[d] Center of Research Excellence in Nanotechnology and Chemical Engineering Department, King Fahd University of Petroleum & Minerals, Dhahran 31261, Saudi Arabia

ARTICLE INFO

Keywords:
Advanced oxidation process
Clay modification
Dye degradation
Sonocatalytic degradation
SnO_2

ABSTRACT

The study on the removal of rhodamine B under ultrasonic-assisted oxidation or called as sonocatalytic oxidation using tin oxide-immobilized onto montmorillonite (SnO_2/MMT) has been investigated. A hydrothermal synthesis was used for preparing the immobilized SnO_2 nanoparticles into montmorillonite structure, and the as-synthesized material was characterized using X-ray diffraction, gas sorption analysis, UV–vis diffuse reflection spectroscopy (UV–vis diffuse reflectance spectroscopy), scanning electron microscopy, and transmission electron microscopy techniques. The kinetics study of the sonocatalytic-assisted oxidation was performed by the comparison with SnO_2 and MMT, and in order to discover the kinetic characteristics of the sonocatalytic oxidation, varied condition such as the effect of initial concentration of rhodamine B, pH, the addition of H_2O_2 were examined. The proposed kinetic model revealed that the degradation obeys the apparent first-order rate kinetics. Refer to the dependence of the kinetics reaction to the initial concentration rhodamine B and H_2O_2 concentration, it is noted that the reaction fit with the Langmuir and Okitsu model suggesting that the sonocatalytic mechanism is influenced by active interface interaction for the cavitation and radical formation as the main operational parameters. pH of the solution directly influences the initial rate of the reaction as the effect of zeta potential of the surface. Reusability study revealed that the catalyst maintains the stability until 3 cycles utilization with the maximum degradation efficiency of ~100 % under the condition of ultrasound frequency of 40 W, 68 kHz, catalyst dose of 0.5 g/L, and reaction time of 2 h.

1. Introduction

Wastewater containing dyes are usually found from some industries such as textiles, printing, and some home-creative industries and often create severe environmental pollution. The difficulties in dye removal of the wastewater sometimes leads for discharging non- or not-completely treated wastewater into environmental water bodies. Dyes are the most important class of synthetic organic compounds with some negative effects such as irritating properties, carcinogenic and destroying aquatic environment [1]. Thus, years of researches develop treatment methods that are more effective in eliminating dyes from the wastewater. Sustainable, low-cost, and efficient are the essential properties of the technique for applicability in industries, including small scale industries. Considering the persistence characteristics of dye compounds, which generally consist of aromatic and stable organic compounds, catalytic oxidation is still a powerful technique among some mentionable methods. Complete oxidation will give mineralization as the main route of the treatment without any further arrangements for the clean technology [2,3]. The catalytic oxidation itself, can be conducted under some intensification process such as electrocatalytic, photocatalytic, and ultrasound or commonly called as sonocatalytic technique. The combination of procedure and catalyst activity plays an important role in the degradation mechanism and its efficiency [4,5]. Among various combinative processes, the ultrasonic-assisted degradation of organic compounds is a promising technique that was reported to be effective due to its simple equipment, high efficiency, stable operation, safety and no secondary pollution [6,7]. In such cases, photocatalytic degradation over a kind of material/ nanomaterial showed higher effectiveness compared to the sonocatalytic process, but it can also in reverse for the other cases. The effectiveness of sonocatalytic and photocatalytic process for dye degradation depends on factors such as the photocatalyst/catalyst, dye, irradiation time,

* Corresponding author.
E-mail address: isfatimah@uii.ac.id (I. Fatimah).

https://doi.org/10.1016/j.jwpe.2020.101418
Received 21 January 2020; Received in revised form 22 May 2020; Accepted 28 May 2020

catalyst dosage, pH etc. Some papers reported the higher degradation efficiency of sonocatalytic process rather than photocatalytic process, for example the degradation of methylene blue over TiO_2–CNT catalysts and the degradation of reactive black with core–shell nanocrystal [8,9].

Metal oxide semiconductors such as TiO_2, SnO_2, ZnO, ZrO_2 showed the activity for the sonocatalytic process refer to capability for electron promotion at the valence band (e_{cb}^-) into the conduction band (CB), leaving a hole h_{vb}^+ and producing radicals for further oxidation process of organic compounds [10,11].

Particularly, tin oxide (SnO_2) is the potential candidate for semiconductor for use as catalysts due to its bandgap energy, and less toxicity. Several researches explored the capability of SnO_2 in sonocatalysis and photo-sonocataysis [12,13]. However, the stability of SnO_2 and low efficiency due to its large bandgap (3.6 eV) and high recombination rate of electron-hole pairs restricts the use of SnO_2 as an efficient sonocatalyst. In order to recover these problems, nanocomposites formation of SnO_2 has been attempted instead of its structural modification [12]. Previous researches reported the use of multiwalled carbon nanotube (MWCT), graphene, zeolite and some porous solids for sonocatalytic and photocatalytic activity enhancement [14,15]. Previous research on cyproflaxine and methyl green degradation over sonocatalytic process conducted by TiO_2/montmorillonite suggested that montmorillonite structure provides effective surface and support for the TiO_2 as an active catalyst by high specific surface area [16,17]. The resulting nanocomposites showed good capability to facilite the oxidation-reduction mechanism by the semiconductor active site by providing adsorption-desorption mechanism. Within these schemes, immobilizations of SnO_2 into clay structure, including bentonite or montmorillonite were reported as promising composites for catalytic oxidation reactions [18]. To our knowledge, the study on synthesis of SnO_2/Montmorillonite for sonocatalytic application has not been reported.

Refer to the potency of smectite clay modification, this research attempted to prepare the composite of SnO_2 with montmorillonite (furthermore called as SnO_2/MMT) and studied its catalytic activity in sonocatalytic degradation of dye. As a dye model, rhodamine B (RhB) was chosen due to its abundantly used in some textile industries. Research highlights the use of hydrothermal technique as a different method with were reported from some previous research. Physicochemical characterization techniques consist of x-ray diffraction (XRD), gas sorption analysis, field emission scanning electron microscope-energy dispersive x-ray (FESEM-EDS), and transmission electron microscopy (TEM) were employed for the study. Further, it was subjected toward sonocatalytic activity studies for the oxidation of RhB in varied condition.

2. Materials and methods

2.1. Materials

Montmorillonite sample was collected from Pacitan, East Java, Indonesia. The sample was activated by refluxing in 2 M of sulfuric acid for 4 h followed by washing using water until the filtrate was neutral (pH 6–7). SnO_2/MMT nanocomposite was prepared by mixing an aqueous suspension of montmorillonite (5 g in 250 mL) with precursor solution made by mixing of stannic chloride solution with NaOH at the Sn/$^-$OH molar ratio of 1:2 followed by stirring for 4 h. The mixture of the suspension and precursor solution was made by setting 20 wt% of Sn percentage in the targeted composite. The mixture was stirred magnetically for 4 h before then hydrothermally aged in autoclave at 150 °C overnight. The precipitate obtained was washed using 3 L of aquadest, dried at 80 °C for 24 h and calcined at 600 °C for 2 h. For comparative studies, SnO_2 nanoparticles were also synthesized by the reaction between stannic chloride dihydrate and sodium hydroxide at the Sn/$^-$OH molar ratio of 1:2 in the aqueous solutions. The mixture was stirred for 4 h at room temperature, and the resulting precipitate was filtered, washed and dried at 80 °C for 24 h. Finally it was calcined at 600 °C for 2 h [19].

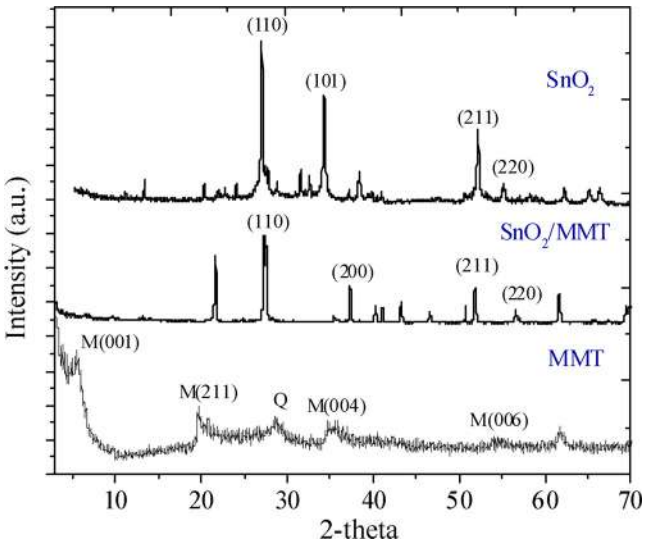

Fig. 1. XRD pattern of materials [M: montmorillonite, Q: quartz).

2.2. Characterization

Characterization of the samples was employed by x-ray diffraction analysis (Rigaku Miniflex-600, Tokyo, Japan). Ni-filtered Cu-Kα with the voltage of 40 kV and 20 mA current was utilized. The surface profile consists of specific surface area, pore volume, and pore radius parameters were determined by N_2 adsorption-desorption experiment using NOVA 1200e gas sorption analyzer. For each adsorption experiment, liquid N_2 at the temperature 77 K was utilized. The specific surface area of materials was calculated based on Brunair-Emmet-Teller (BET) method, while the pore volume data was determined using Barrett, Joyner, and Halenda (BJH) method. FTIR Spectroscopy was carried out using Perkin Elmer–ATR (Singapore). Surface morphology was studied by using FESEM taken on a JX-JEOL electron microscope. The photoluminescence spectrum was recorded with Fluorescence spectrophotometer (JASCO V760, Tokyo, Japan).

2.3. Catalytic activity test

Sonocatalytic degradation of RB was employed by an ultrasonic probe with a frequency of 40 kHz and ultrasonic power of 68 W (Delta DH68H, Taiwan). For each experiment, 0.5 *g* of the catalyst was added into 1 L of RhB solution, and then the sonicator probe was immersed into the mixture. The sampling was conducted at the interval of time by collecting the solution and centrifuged before analyzed using UV–vis spectrophotometric method. A calibration curve of rhodamine B at the desired concentration range was employed by measuring the absorbance at 554 nm using a HITACHI U2080 UV–vis spectrophotometer. Degradation efficiency (DE/%) was calculated based on the change of RhB concentration before and after treatment using the following Eq. (1):

$$DE(\%) = \frac{[C_0 - C_t]}{C_0} x\ 100\,\% \quad (1)$$

Identification on the presence of dye degradation was conducted by liquid chromatography-mass spectrometry (LCMS). The specified operational condition consists of a mixture of methyl alcohol and water (50:50, v/v) as the mobile phase with the flow rate of 0.8 mL·min^{-1}, and the injection volume of 20 μL were applied on a HITACHI LCMS instrument. MS analysis was performed on spray voltage of 3.5 kV; capillary temperature, 325 °C; capillary voltage, 50 V, tube lens 120 V,

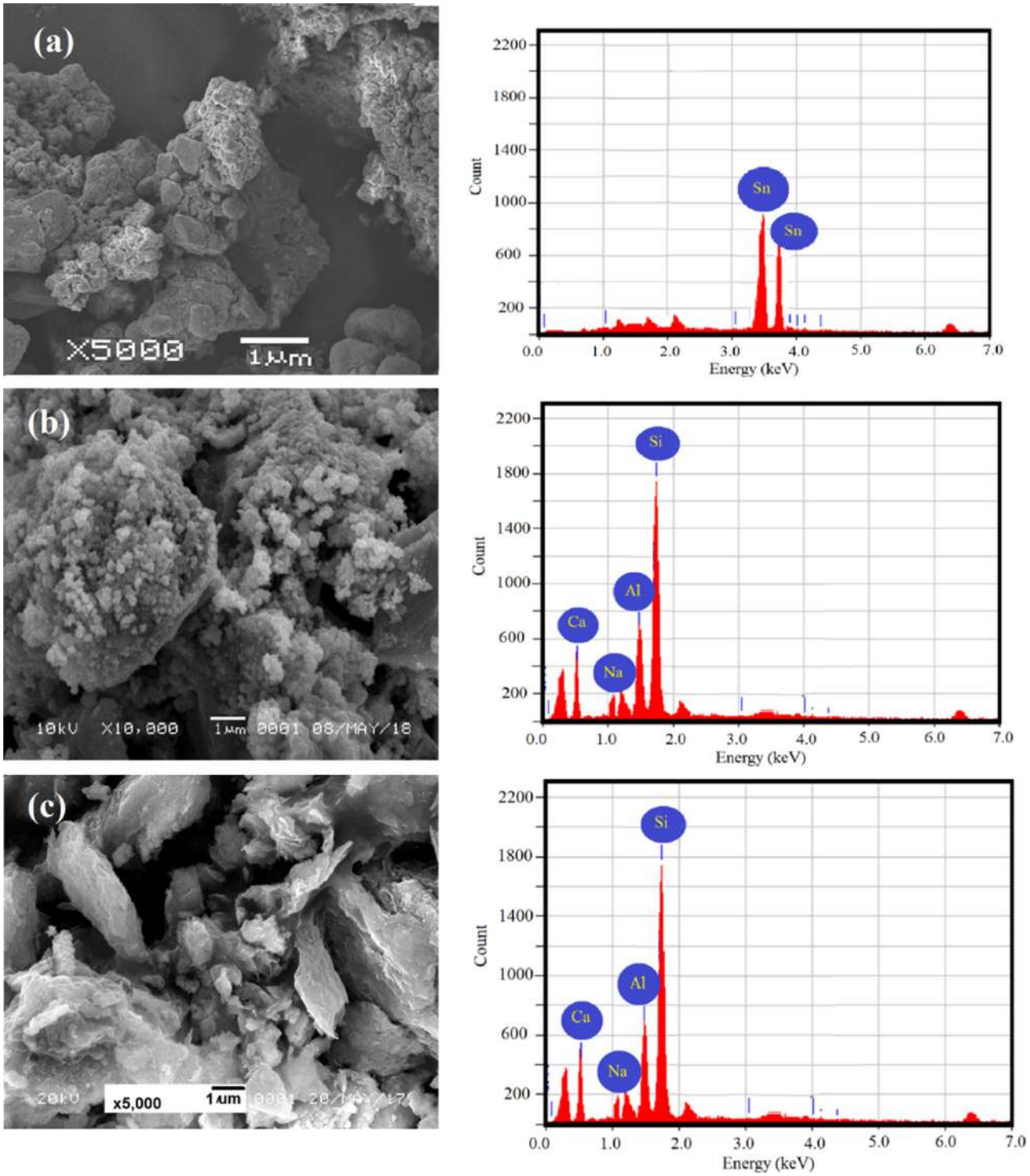

Fig. 2. SEM-EDS profile of (a) SnO_2 NPs (b) SnO_2/MMT (c) MMT.

and the detection of the mass range was ranging at 50–600 *m/z*.

Total organic carbon (TOC) was measured by US Environmental Protection Agency (USEPA) Method 415.3. Reusability of the catalyst was tested after each recycling process. The recycling was performed by filtering the catalyst after use, washing using ethanol and dried at 200 °C for 2 h.

3. Results and discussion

3.1. Physicochemical character of material

The crystalline structures of SnO_2, MMT and SnO_2/MMT composites were confirmed by XRD patterns (Fig. 1). The diffraction peaks at 26.9°, 37.9°, 39.58°, and 51.9° of SnO_2 and SnO_2/MMT samples are found and correspond to (110), (101), (200), and (211), with the extension of peak at and 54.7° which corresponding to (002) planes of tetragonal rutile SnO_2 (JCPDS 41-1445) respectively. Meanwhile, MMT presents the

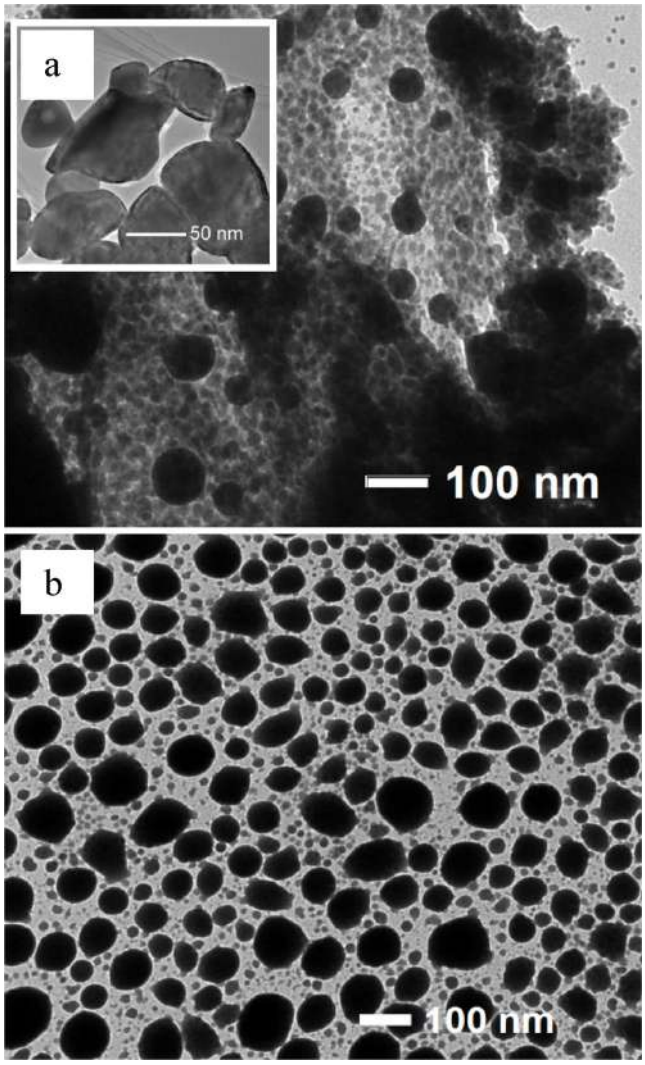

Fig. 3. TEM profile of SnO_2 NPs and SnO_2/MMT (inset: HRTEM profile).

Table 1
Elemental analysis of MMT, SnO_2, and SnO_2/MMT.

Compound	Amount (%wt.)		
	MMT	SnO_2	SnO_2/MMT
K_2O	0.05		–
Na_2O	1.63		–
Al_2O_3	35.34		22.13
SiO_2	62.64		56.07
CaO	0.34	0.4	–
SnO_2	nd	99.6	21.80
	100	100	100

characteristic peaks at 5.55, 19.7, 27.7, 35.5 and 54.6° as identification of (001), (211), (004) and (006) of montmorillonite structure. The peak at 27.4° is the indication quartz (Q) contained in the montmorillonite sample, since the material is natural mineral which is available and inseparable with silica materials. The (001) peak of montmorillonite at 5.55° [M(001)] represents the basal spacing d_{001} of 13.5 nm. It is also concluded that the immobilization of SnO_2 is not representing the pillarization of SnO_2 into interlayer structure of MMT since the (001) peak is disappeared rather than shifted into a left side or indicating the increasing the basal spacing. The pattern is similar with previous research on SnO_2 immobilization into bentonite [18] with the Sn percentage ranging at 10 − 30%. Using Debye-Scherrer equation (eq.2), the crystallite size of SnO_2 NPs on SnO_2/MMT surface is calculated to be 54.6 nm.

The presence of SnO_2 NPs in the composite is also characterized by SEM-EDX profile as well as TEM profile (Figs. 2 and 3). A relative rougher surface was expressed by SnO_2/MMT respect to the MMT's surface which implies a layered structure as surface characteristic of smectite clay. Refer to the surface profile of SnO_2 NPs, these rougher and irregular particles on surface are the identification of the supported SnO_2. Based on EDS spectra, the SnO_2 content in the composite was calculated to be 21.8 %wt. (Table 1) which is slightly higher compared with targeted content (20 % wt.). In addition, TEM profile of SnO_2/MMT (Fig. 3) with HRTEM profile (inset) presents the non-homogeneous spherical particles of SnO_2 ranging at 40 − 60 nm in size meanwhile, the SnO_2 NPs shows the bigger particles in range. The particle size range is fit with the crystallite size measured by XRD calculation.

To ensure the presence of SnO_2 interaction with the support, XPS analysis was conducted, and the results are presented in Fig. 4. The survey scan spectrum depicted in Fig. 4a demonstrates the presence of Si, Al, Fe, Sn, O and Na peaks confirming the main component of montmorillonite and the supported SnO_2. The deconvoluted O1 s spectrum (Fig. 4b) demonstrated the two peaks centered at 486.9 and 485.8 eV which belong to the Sn^{4+}-O and Sn^{2+}-O bonds. This suggests that the partial transition of Sn^{4+} to Sn^{2+} occurred [20,21]. The deconvolution of Sn 3d spectrum shows two peaks at 530.3 and 531.7 eV (Fig. 5c), which belong to the Sn—O and OH— bonds, as the proof of SnO_2 structure in the composite. Furthermore, Fig. 4c depicts two peaks of the Sn $3d_{5/2}$ and Sn $3d_{3/2}$ spin-orbit at at 486.9 and 495.3 eV, respectively. It is also noted that the distance between the two peaks is 8.4 eV, which confirms the formation of Sn^{4+} oxidation state in SnO_2.

The change in surface profile from MMT into SnO_2/MMT is in line with the surface parameters listed in Table 2 which are calculated from adsorption-desorption isotherm (Fig. 5). The SnO_2 immobilization affected to increase specific surface area of MMT from 76 m^2/g to 128 m^2/g, corresponding with the increasing pore volume from 1.02 × 10^{-2} cc/g to 1.90 × 10^{-2} cc/g. The parameters are higher compared with SnO_2 NPs as an indication of the formation of porous structure on the surface which is important for heterogeneous catalysis mechanism.

To estimate the band gap energy of the composite, UV-DRS analysis was performed (Fig. 6). The diffuse reflectance spectra of the samples were evaluated using the Tauc plot equation of the measured reflectance according to the following Eq. (2):

$$(\alpha h\nu)^2 = A(h\nu\text{-}Eg) \quad (2)$$

where α, ν, E_g, and A are the absorption coefficient, light frequency, bandgap energy, and a constant, respectively. The band gap energy was obtained by extrapolating the linear portion of the $(\alpha\ h\ \nu)^2$ curve versus hν to zero, and from this, the estimated bandgap energies of the SnO_2 and SnO_2/MMT obtained from the Tauc plot are, 3.54 and 3.6 eV respectively. The increasing E_g of SnO_2 by supporting onto MMT suggesting the effect of smaller particle size which furthermore respect to the stabilization of the excited electron.

3.2. Catalytic activity of SnO2/MMT

Kinetics of RhB sonocatalytic degradation over SnO_2, SnO_2/MMT and MMT is depicted at Fig. 7. The kinetic plots imply that both SnO_2 and SnO_2/MMT show the degradation activity as demonstrated by the decreasing RhB concentration effectively at time range of 0 − 120 min, meanwhile MMT does not show significant effect to C/C_o at the same time. The data suggests that the presence of SnO_2 as catalyst active material plays role in the degradation mechanism, at the meantime, the slightly decreasing RhB concentration over MMT is occurred by adsorption mechanism. Even though in the system H_2O_2 was added, but there is no significant change in RhB concentration.

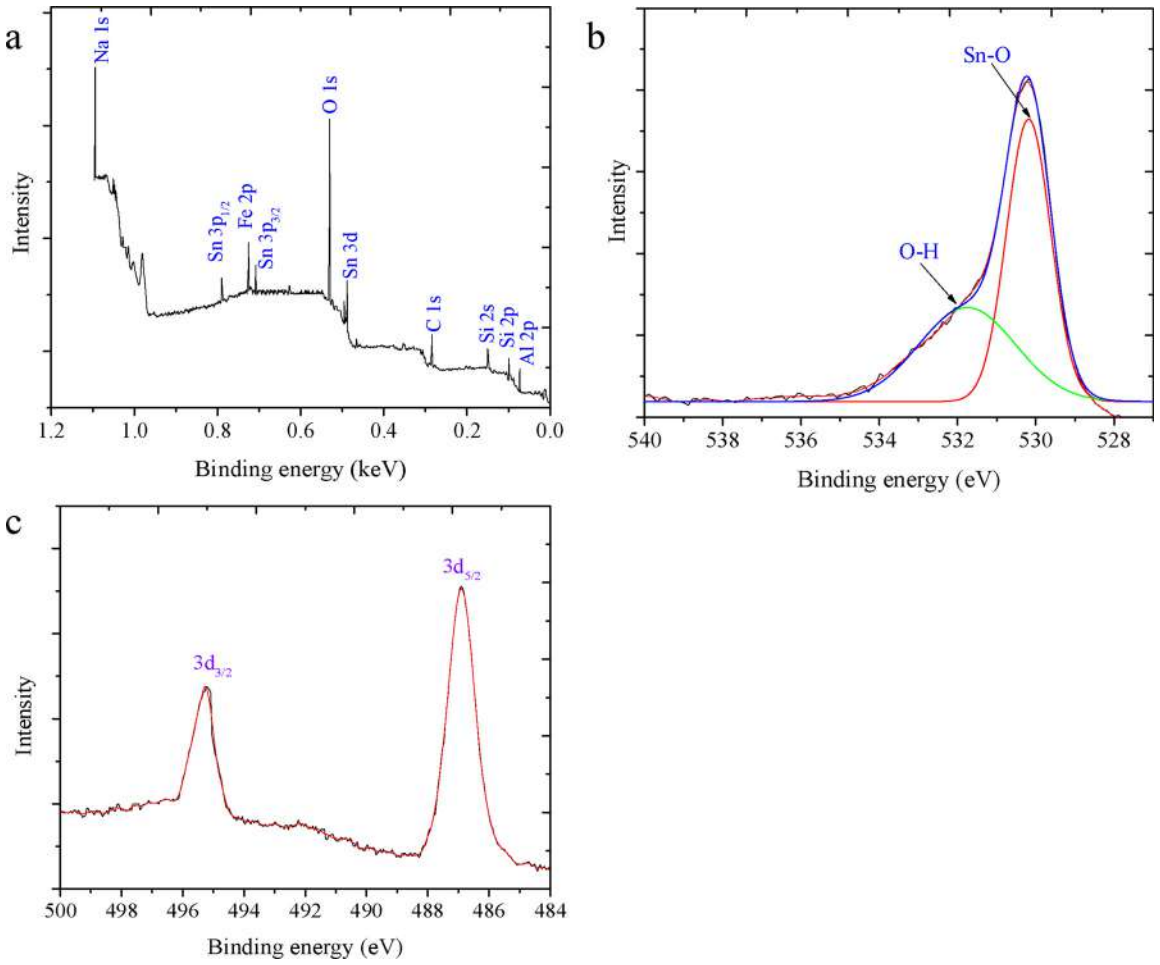

Fig. 4. (a) XPS spectra of (a) survey scan (b)O 1s (c) Sn 3d of SnO_2/MMT.

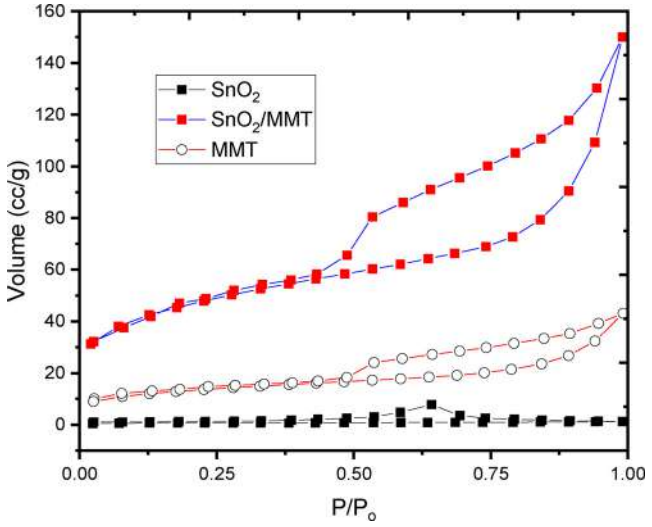

Fig. 5. Adsorption-desorption profile of materials.

Table 2
Surface profile of MMT, SnO_2, and SnO_2/MMT.

Catalyst	BET specific surface area (m^2/g)	Pore volume (cc/g)
SnO_2/MMT	128	1.90×10^{-2}
SnO_2	21	8.12×10^{-3}
MMT	76	1.02×10^{-2}

The change in RhB concentration describes the presence of cavitation by the catalytic active sites from SnO_2 which produce efficient amount of hydroxyl radicals to degrade RhB. The interaction among ultrasound and active site creates a hot spot and furthermore, it generates strong oxidizing conditions by the interaction between radicals formed and the hydroxyl radicals (H· and · OH) coming from H_2O_2 as oxidant by following mechanism [14,22]:

$$SnO_2 +))) \longrightarrow e^- + h^+$$

$$e^- + O_2 \longrightarrow O_2^{\cdot -}$$

$$e^- + {}^-OH \longrightarrow {}^{\cdot}OH$$

$$h^+ + H_2O \longrightarrow {}^{\cdot}OH$$

$${}^{\cdot}OH + O_2^{\cdot -} + \text{Dye} \longrightarrow CO_2 + H_2O$$

Schematic representation of sonocatalytic mechanism is presented in Fig. 8.

Investigation on the kinetics of RhB degradation was studied by applying two kinetics equations; pseudo-first order kinetics and pseudo-second order kinetics with following eq. (3–4):

$$ln\frac{C_t}{C_0} = -kt \tag{3}$$

$$\frac{1}{C_t} = kt + \frac{1}{C_0} \tag{4}$$

and the calculated parameters are presented in Table 3.

From comparison on the use SnO_2/MMT and SnO_2, it is also notably concluded that the degradation efficiency, initial rate and kinetics

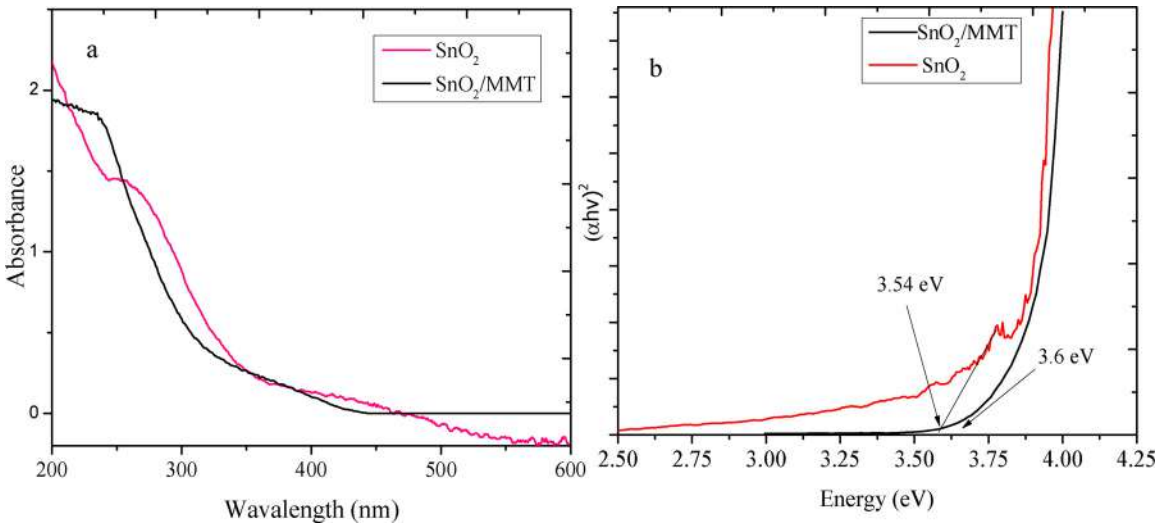

Fig. 6. (a) UV-DRS spectra (b) Tauc plot of SnO_2 and SnO_2/MMT.

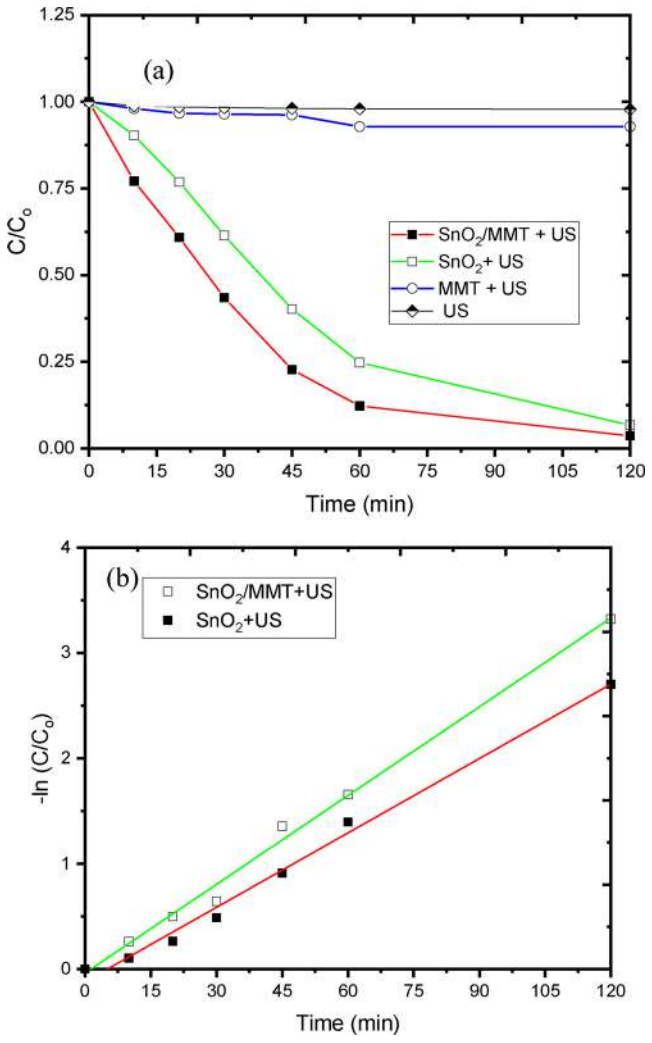

Fig. 7. (a) Kinetics of RhB sonocatalytic degradation over SnO_2 and SnO_2/MMT (b) pseudo-first order plot of the kinetics (C_{RhB0} = 20 mg/L, catalyst dosage = 0.5 g/L).

constant as shown by the slope of the plot over SnO_2/MMT are higher compared to SnO_2 (Table 3). The R^2 parameters suggest that the data obeys pseudo-first order kinetics since the R^2 of pseudo-first-order kinetics model is higher than of pseudo-second-order kinetics model.

Using the pseudo-first-order plot, the apparent kinetics constant (slope) of the reaction over SnO_2/MMT and SnO_2 are 0.032/min and 0.020/min, and are consequently comparable with the initial rate 0.60 mg/L.min and 0.38 mg/L.min, respectively. By using the consideration that SnO_2 is active site for degradation mechanism, turnover number (TON) of the reaction was calculated based on the percentage of RhB degraded per mass of SnO_2 in the catalyst, and the values are calculated to be 2.74 mg/wt%.L and 0.38 mg/wt%.L, respectively. The values demonstrate the relevance of SnO_2 supporting into MMT structure, which possibly correlated with the preserved specific surface area of the composite form to enhance the efficiency by the participation of adsorption in the mechanism.

The data indicated that the kinetics rely on initial concentration of RB, and it presumably that the surface interactive occurs at the bubble-liquid interface. At the interface spot, amount of hydroxyl radicals can be denoted as in a constant amount so the equation of reaction rate (5):

$$R = k\,[RhB][OH], \quad (5)$$

Which can be simplified expressed as (6):

$$R = k_{app}\,[RhB], \quad (6)$$

With $k_{app} = k.[OH]$

Similar kinetics profile and possible mechanism was similar with sonocatalytic degradation of RhB by SnO_2 and TiO_2 reported by previous works [23–25].

The identification of degradation mechanism in the sonocatalysis process was studied by LCMS analysis giving the data presented at Fig. 9. The chromatograms of initial and treated solution for 30 and 60 min. show the degradation as identified by some new peaks of treated solutions respect to the chromatogram of initial solution. In addition the mass spectra of treated solution exhibit the fraction with *m/z* of 362, 274, 228, 216, 172, 168, 148, 122, 104, 90, 76, and 74 as identification of degradation products. The identified molecules from these mass spectra were products from N-de-ethylation and decarboxylation (*m/z* 274), oxalic acid ($C_2H_2O_4$, *m/z* 90), 3-(diethylamino)phenol ($C_{10}H_{15}NO$, *m/z* 168), 2-vinylbenzoic acid ($C_9H_8O_2$, *m/z* 148), 2-(2,5-dihydroxypheny)acetic acid ($C_8H_8O_4$, *m/z* 168), malonic acid ($C_3H_4O_4$, *m/z* 104), and formic acid (CH_2O_2, *m/z* 46). These observed intermediates are the proof of degradation via N-de-ethylation, de-alkylation, de-amination, de-carboxylation, de-hydration, cleavage of the chromophore, and the breakage of ring structure refer to [26–28].

The proof of degradation is also identified by the TOC removal at varied initial concentration of RhB by the treatment for an hour as

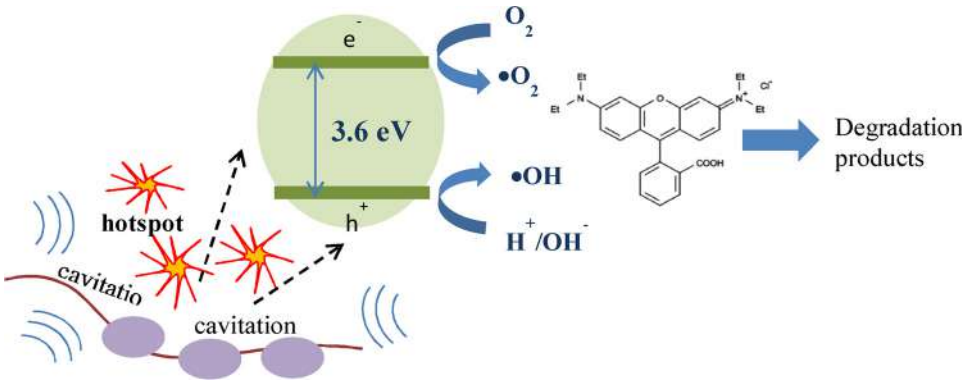

Fig. 8. Mechanism of sonocatalytic degradation of RhB.

Table 3
Calculated parameters of kinetics data.

Catalyst	Initial rate (mg/L.min)	Pseudo-first order kinetics model		Pseudo-second order kinetics model		DE (%)	TON (mg/wt%.L)
		R^2	Equation (k)	R^2	Equation (k)		
SnO_2/MMT	0.60	0.9990	$\ln C_t = -0.032t - 0.042$	0.9310	$\frac{1}{C_t} = 0.063t + 0.702$	90	2.74
SnO_2	0.38	0.9960	$\ln C_t = -0.020t - 0.075$	0.9530	$\frac{1}{C_t} = 0.036t + 0.819$	81	0.41

presented in Fig. 10. TOC removal ranging at 35–58 % is demonstrated from initial RhB concentration of 5 − 50 ppm. The TOC represents the removal of organic content over oxidation mechanism, which consist the released produced gas. The reducing TOC removal at the increasing initial concentration of RhB is related with the higher amount of intermediates products in more concentrated solution.

3.3. Kinetics model of sonocatalytic reaction

As the RhB degradation obey pseudo-first order kinetics, the degradation rate is depending on the initial concentration of RhB. Effect of initial concentration on initial rate can be used for determining the effect of surface interaction during cavitation. Kinetics plot on varied initial RhB concentration is depicted in Fig. 11.

Refer to previous sonocataytic process, the decomposition of dye molecule occurs in the interface region of the cavitation bubbles. Since the concentration of OH radicals is adequate for the effective reaction at the interface and cavitation zone after the bubble collapse and the temperature is also high, the oxidative and thermal decomposition will be quickly occurred in this zone.

Taking into account that interaction of interface and radicals play an important role in the kinetic, refer to [29], Langmuir adsorption in the reaction mechanism is assumed to be occurred and the model can be applied with following eq. (7):

$$r_0 = \frac{kKC_o}{1 + KC_0}, \tag{7}$$

which can be converted into a linear form eq. (8):

$$\frac{1}{r_0} = \frac{1}{kKC_0} + \frac{1}{k} \tag{8}$$

With r is the initial dye degradation rate (mg/L.min), k is the apparent rate constant (min^{-1}), K is the equilibrium constant (L/mg) and C_0 is the initial dye concentration (mg/L). K is the equilibrium constant, which corresponds to the ratio of the adsorption to desorption rate constants of dye onto an effective reaction site.

Another model which is modified Langmuir model, called as Okitsu's model was also tested with following Eq. (7):

$$C_0 = k\left(\frac{C_0}{r}\right) - \frac{1}{K} \tag{a}$$

Based on the kinetics data presented with plot at Fig. 11a, the Langmuir and Okitsu models are presented in Fig. 11b and c, and the calculated parameters are listed in Table 4.

Due to the R^2 parameters, it is concluded that both models are fit with the kinetics data suggesting that these obey the basic assumption of Okitsu's model. In short, the pollutant molecules in the interface are proportional to the initial concentration in solution, the adsorption-desorption equilibrium occurs in between interfacial zone and bulk state of the catalyst, high concentration of radicals are existed for the fast degradation [22].

3.4. Effect of H2O2 concentration

Based on the kinetics results, the sonocatalytic degradation kinetics under varied H2O2 concentration was then studied, and the results are illustrated in Fig. 12. As shown, the pattern expressed the increasing degradation rate at increasing H_2O_2 ranging from 0 to 2×10^{-3} M but then maintained at further increasing concentration. High concentrations of H_2O_2 will adversely affect the efficiency of photocatalytic reaction by the radical scavenger and holes (h^+) scavenger according to following reactions:

$$H_2O_2 + HO^{\cdot} \rightarrow H_2O + HO_2{}^{\cdot}$$

$$HO_2{}^{\cdot} + HO^{\cdot} \rightarrow H_2O + O_2.$$

3.5. Effect of pH of the solution

From the kinetics plot at Fig. 13, it is concluded that the degradation efficiency of RhB is highly affected by the pH value. Refer to the fitness to L-H kinetics, the degradation mechanism is related to the equilibrium governing the surface interaction between dye, radicals and SnO_2 in the reactin system. Fig. 13a and b show that the degradation reach fastest on pH 4 with the degradation efficiency of more than 98 % and initial rate of 37 mg/L.min. The increase in pH value to 7 until 11 significantly reduces the initial rate. It is noteworthy that the isoelectric point of SnO_2/MMT from zeta potential analysis (Fig. 13c) is pH 4.4, while RhB

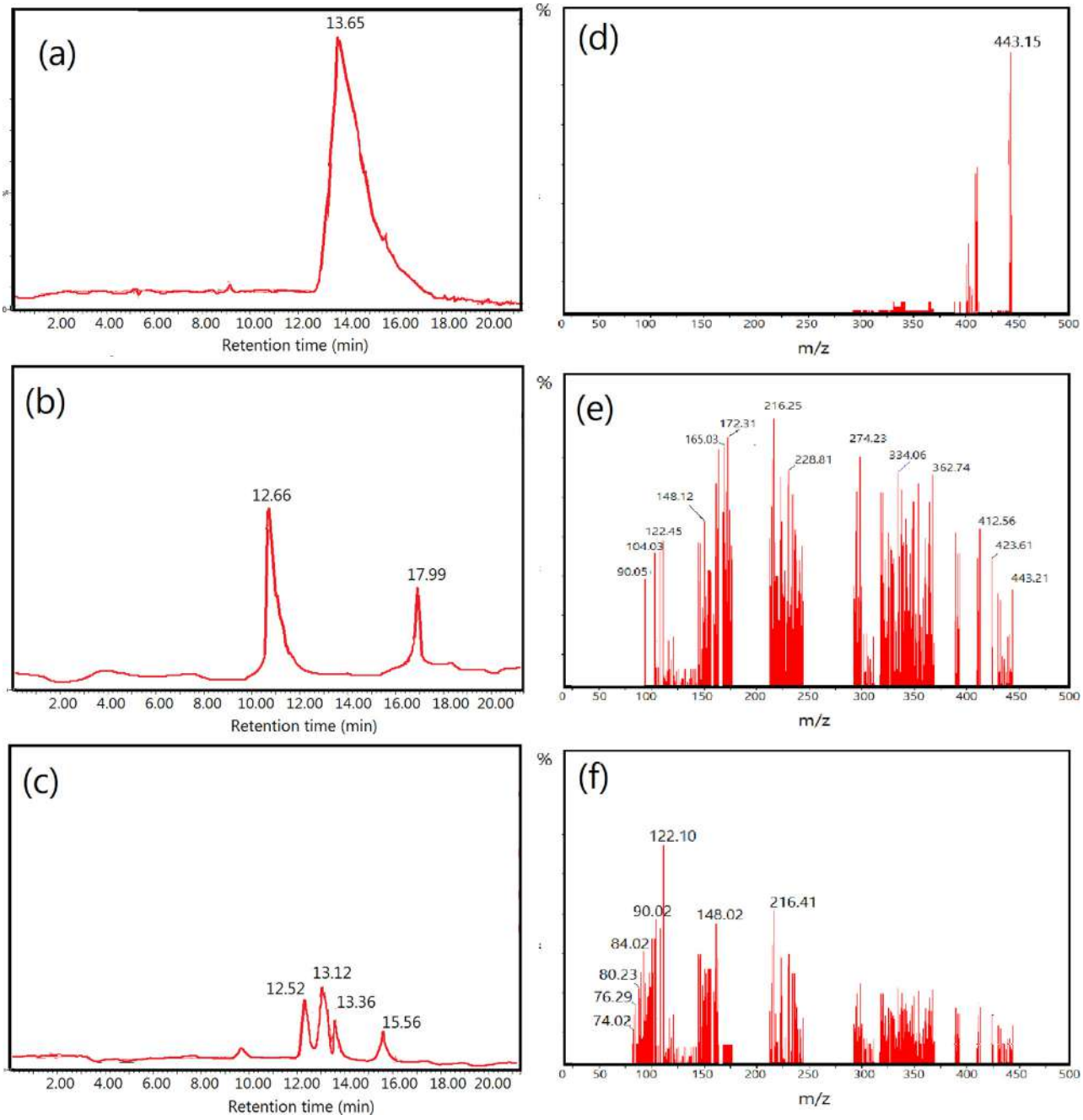

Fig. 9. (a-c) Chromatogram of initial, treated RhB solution for 30 min, and 90 min, respectively, (d-f) Mass spectra of initial, treated RhB solution for 30 min, and 90 min, respectively.

is a cationic organic dye. In the solutions at pH < 4.4, the SnO_2/MMT will be negatively charged and attractive to RhB so the surface interaction will be more effective, but at strong acidic (pH 2), the surface interaction and radicals formation is retarded by the high concentration of proton. On the other hand, the addition alkaline medium at pH > 4.0, the degradation efficiency and rate of RhB over SnO_2 can be enhanced. However, higher concentration of hydroxyl ions (> 4.4) the surface interaction will prevents the degradation mechanism. The more hydroxyl ions in the system is also proven by that even the zeta potential at pH 11 is higher than pH 9 but it gives no significant different in initial rate.

3.6. Effect of radical scavenger

To study the role of ·OH in sonocatalytic degradation, the effect of ·OH scavenging agents (EDTA and isopropanol) on kinetics was examined. The compared kinetic plots with comparative kinetics constant (inset) presented in Fig. 14 shows that both EDTA and isopropanol significantly suppressed the degradation of RhB. The trapped radicals by the scavengers could not later react to oxidize RhB. It is noted that isopropanol is more effective as the scavenger since it reduced kinetic constant compared to EDTA.

In general, the use of SnO_2/MMT for the sonocatalytic degradation of RhB presented in this work is notably similar with other catalyst materials as listed in Table 5. It is worthy to state that SnO_2/MMT shows as a potential material for sonocatalytic degradation of dye.

3.7. Catalyst reusability

Reusability is an important character for the catalyst to be applied

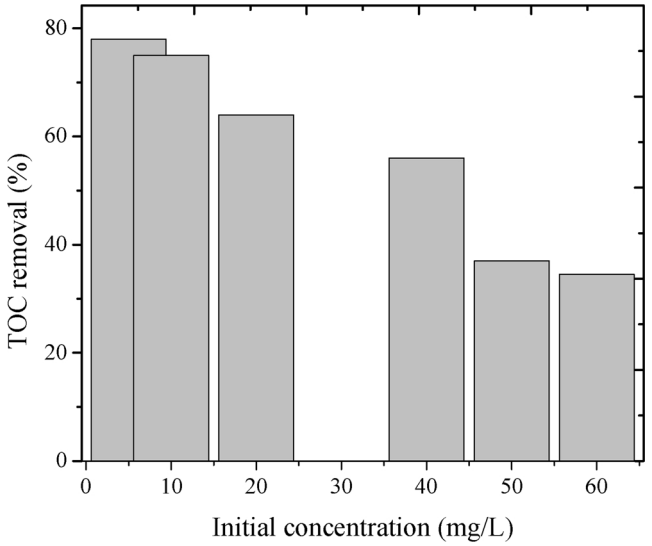

Fig. 10. TOC removal at varied initial concentration of RhB.

in industrial scale. Fig.14 shows the kinetics of RhB degradation by 1st until 6th use on the RhB initial concentration of 50 mg/L and H_2O_2 concentration of 10^{-3} M. The catalyst was recycled by filtering, washing using ethanol and dried after the completion of each cycle.

Table 4
Kinetics parameters of Langmuir and Okitsu models of RhB sonocatalytic degradation kinetics data.

Model	Langmuir	Okitsu
R^2	0.9969	0.9986
k	1.59	1.49
K	48.02	0.022

From the data of DE and initial rate, it is concluded that SnO_2/MMT catalyst is stable until 3rd cycles, and going reduced for the additional cycles. Similar trend in decreasing DE of SnO_2/MMT is also expressed by SnO_2 with the highlight that SnO_2/MMT exhibits higher value in all cycles. The comparison suggests that the reducing activity is related with the loss activity of SnO_2 after use, which is also confirmed by the comparison on initial rate at all cycles.

The catalytic activity depletion is studied by the change of physicochemical character of the catalyst after uses compared with fresh catalyst. The change in XRD pattern, BET specific surface area, and SnO_2 content are in Fig. 15.

The reflection in Fig. 15a. suggests that the crystallinity and structure of the SnO_2/MMT was maintained after 3rd use as indicated by a relative same intensity of peaks corresponding to the presence of SnO_2. At further uses, the crystallinity went to be reduced as indicated by the broadening almost all reflections of material after 5th and 6th uses.

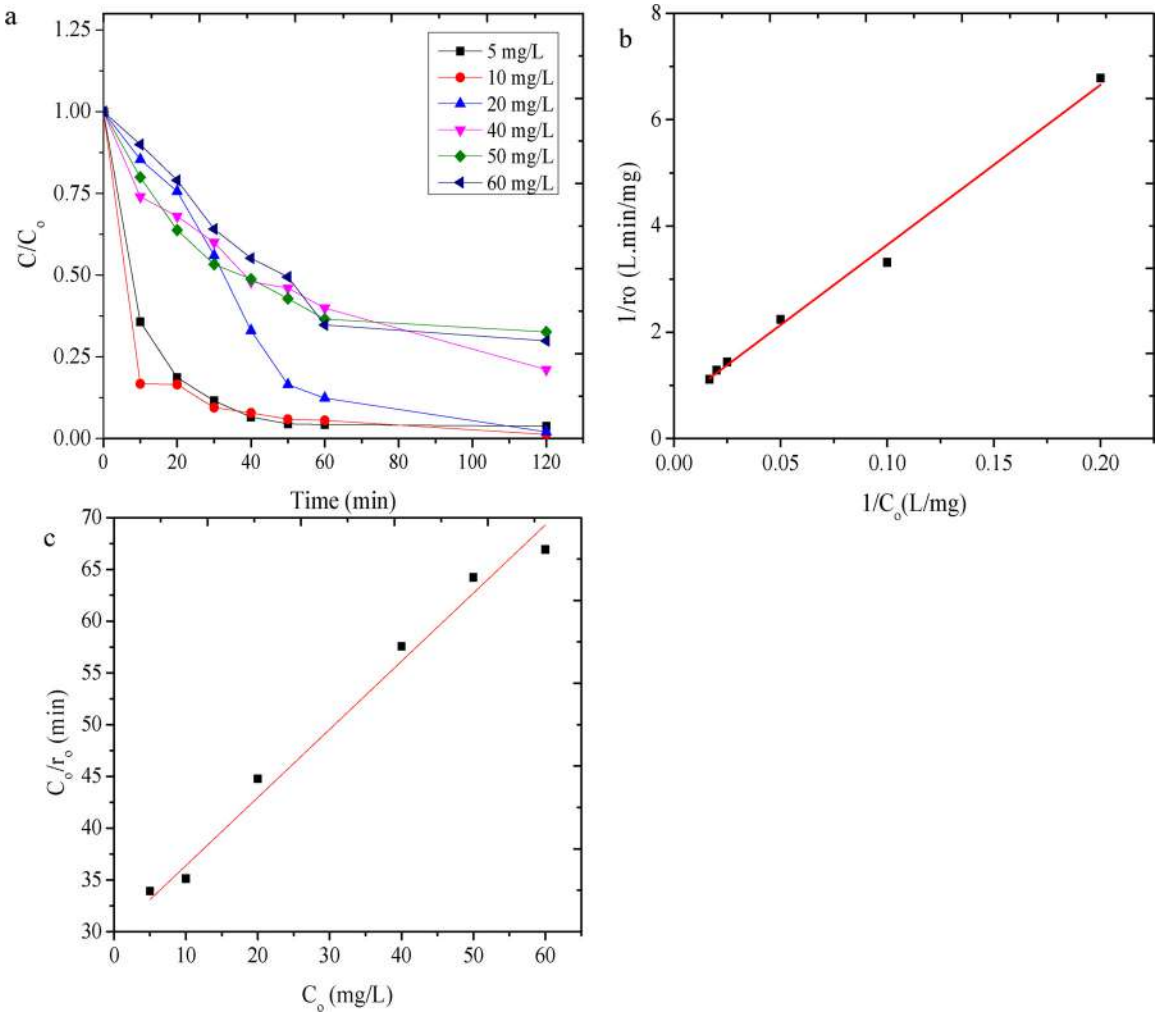

Fig. 11. (a) kinetics plot of RhB sonocatalytic degradation at varied initial concentration of RhB (b) Langmuir plot of the kinetics (c) Okitsu model plot of the kinetics ($C_{catalyst}$ = 0.5 g/L, $C_{H2O2} = 2 \times 10^{-3}$ M).

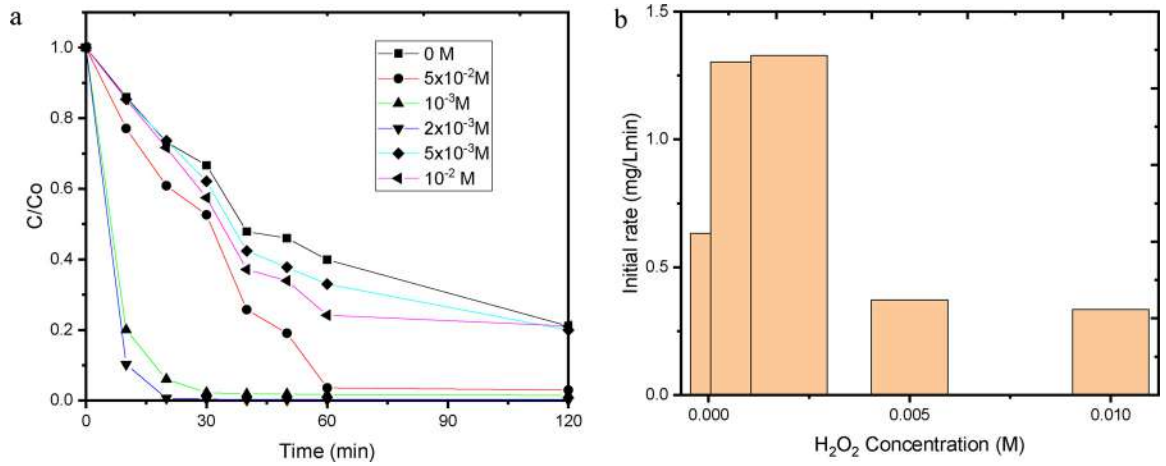

Fig. 12. (a) Kinetics of RhB sonocatalytic degradation at varied H_2O_2 concentration (b) Initial rate of RhB sonocatalytic degradation at varied H_2O_2 concentration (C_{RhB} = 40 mg/L. $C_{catalyst}$ =0.5 g/L).

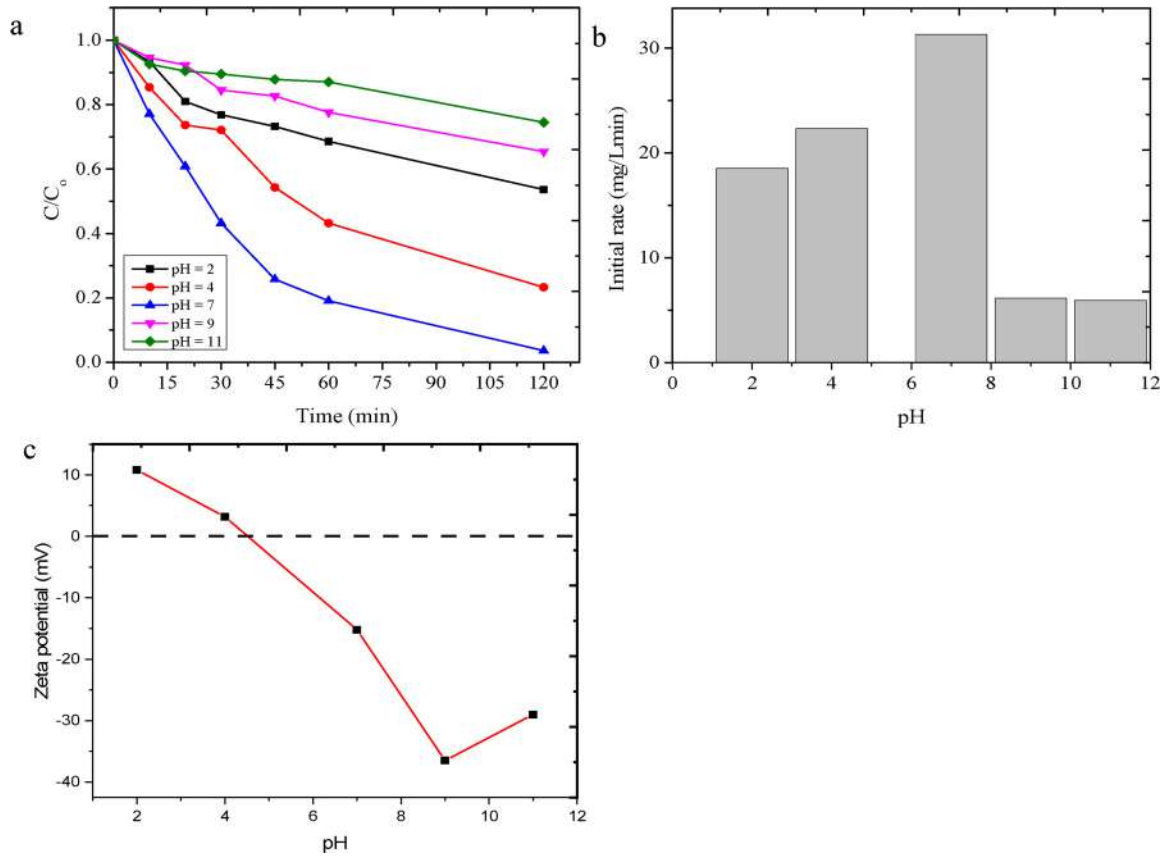

Fig. 13. (a) Kinetics of RhB sonocatalytic degradation at varied pH of solution (b) Initial rate of the kinetics at varied pH of solution (c) zeta potential of SnO_2/MMT at varied pH (C_{RhB} = 40 mg/L. $C_{catalyst}$ =0.5 g/L, no H_2O_2).

These changes are in consistence with the BET specific surface area evolution presented in Fig. 15b, which remarkably confirmed the change of porous structure after 5th 6th cycle of utilization, while the SnO_2 content in all uses remains relatively unchanged. The data imply that the loss of catalytic activity is not respected to the change of material structure rather than the loss of SnO_2 content in the composite. The recycling process including re-calcination affect to composite structure as the support, beside of that the clay structure is vulnerable to electron beam coming from the electron excitation. This phenomenon suggests the role of clay material to reduce potentially damage to the SnO_2 structure as also identified by the higher performance of SnO_2/MMT compared with SnO_2.

4. Conclusion

Degradation of RhB dye by sonocatalytic process using tin oxide-immobilized montmorillonite composite has been reported. SnO_2/MMT exhibits the higher activity for sonocatalytic degradation as shown by the increasing degradation efficiency toward RhB compared to SnO_2 nanoparticles as shown by the higher turnover number and degradation efficiency of the process. The increasing performance is related with the increasing physicochemical character of the material referred to the

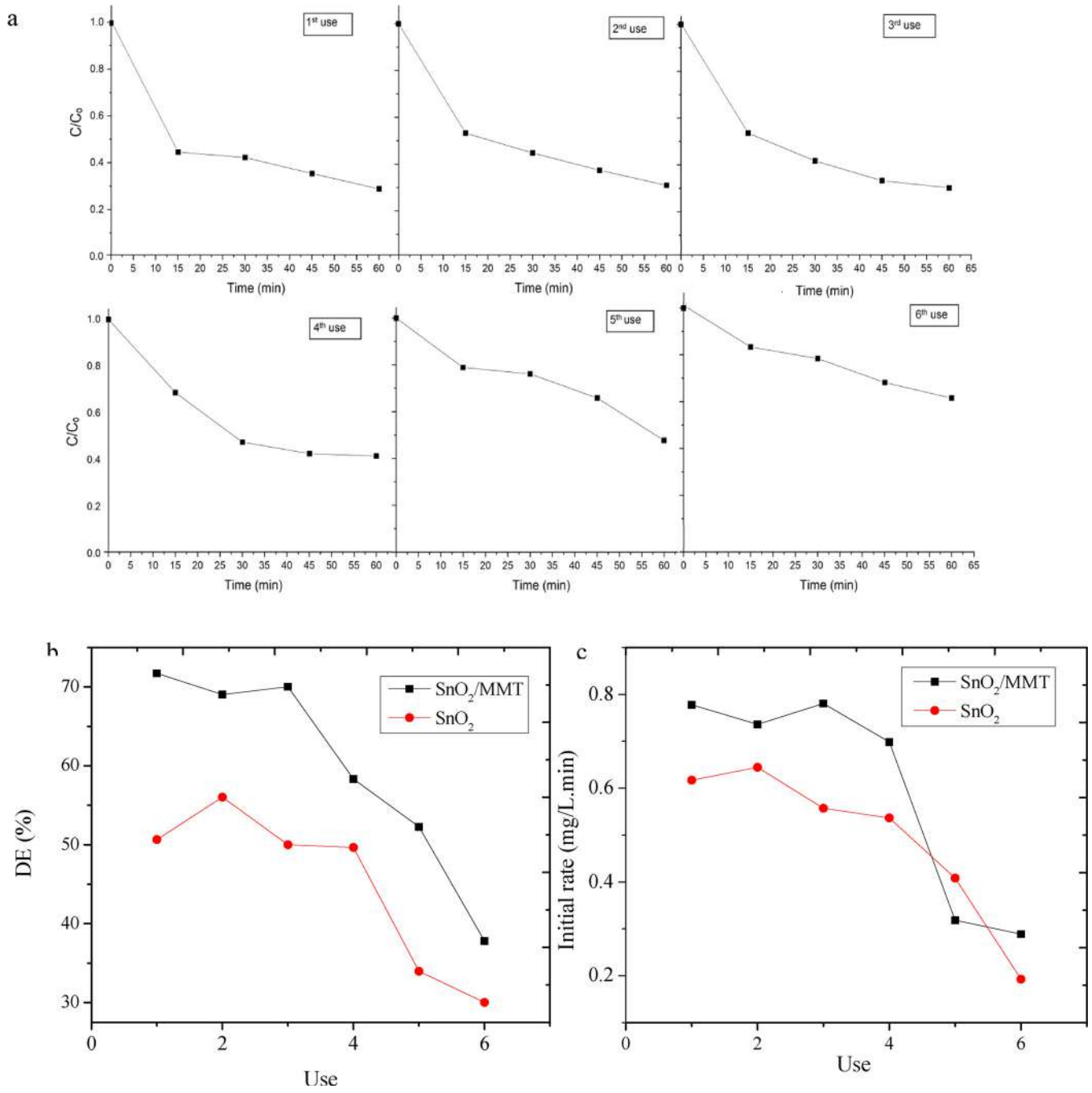

Fig. 14. (a) Kinetics of RhB sonocatalytic degradation at 1st-6th cycles (b) DE at reusability (c) Initial rate at reusability.

Table 5
Comparison on degradation efficiency towards RhB by sonocatalytic degradation using various catalyst.

Catalyst	Condition	DE (%)	Ref
TiO_2 Coated Activated Carbon (TiO_2/AC)	pH 6, temperature 50 °C, ultrasonic frequency (f) = 30 kHz, time of treatment = 60 min.	82.21	[30]
CdS	f = 40 kHz, 100 W	70 %	[31]
TiO_2 nanotube	f = 35 kHz, 100 W, time = 4 h, initial concentration of RhB (C_{RhB}) = 44.9 mg/L	94.6 %	[25]
$LuFeO_3$	f = 60 kHz, T = 40 °C, $C_{catalyst}$ = 4 g L^{-1}, and C_{RhB} = 5 mg L^{-1}	90	[32]
MIL-101(Cr)/RGO/$ZnFe_2O_4$	C_{RhB} = 25 mg/L, C_{H2O2} = 40 mmol/L and pH = 7, $C_{catalyst}$ = 0.75 g/L	90	[33]
Desert Roses (DRs)-ZnO NPs	Frequency of 59 kHz, 40 kHz, catalyst 0.5 g/L, initial concentration 2.5 mg/L	100	[34]
Peat moss-derived biochar	f = 40 kHz and 300 kHz, $C_{catalyst}$ = 0.1/500 mL, C_{RhB} = 100 mg/L	51.8 %	[35]
β-Bi_2O_3	f = 60 kHz, T = 40 °C, $C_{catalyst}$ = 3 g L^{-1}, and C_{RhB} = 5 mg L^{-1}. C_{RhB} = 5 mg L^{-1}, $C_{catalyst}$ = 1 g L^{-1}	987	[36]
SnO_2/MMT	f = 60 kHz, 48 W, $C_{catalyst}$ = 0.5 g L^{-1}, C_{RhB} = 50 mg L^{-1}, H_2O_2 = 2 × 10^{-3} M, 2 h	~100	This research
SnO_2/MMT	f = 60 kHz, 48 W, C_{RhB} = 1 − 20 mg L^{-1}, $C_{catalyst}$ = 0.5 g L^{-1}, C_{RhB} = 50 mg L^{-1}, 2 h	~100	This research

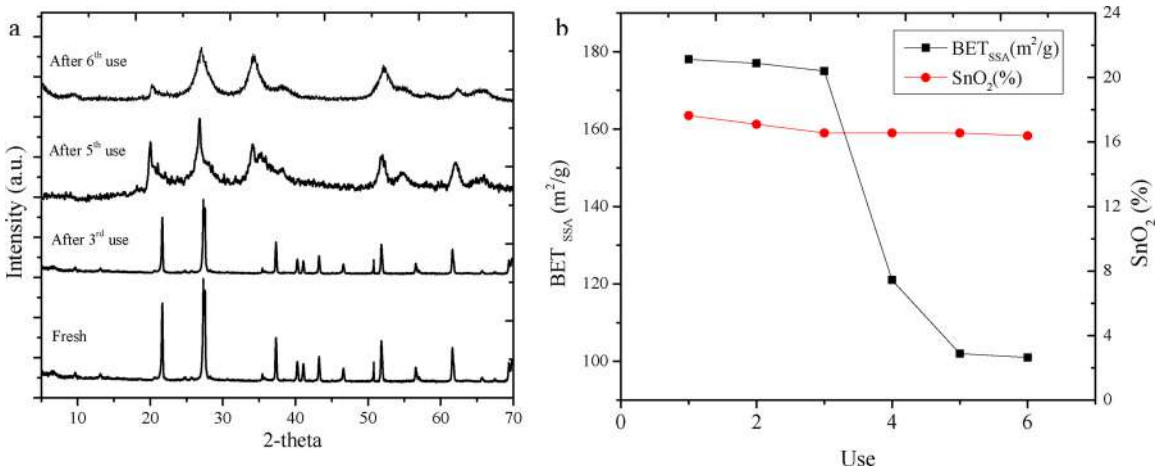

Fig. 15. XRD pattern of catalyst after uses compared to fresh catalyst.

specific surface area, pore volume, particle size of SnO_2 and surface morphology of the material. Furthermore, the study revealed the pH and the initial concentration of dye as important factor for the efficiency. The fitness of the kinetics with Langmuir and Okitsu model represents the role of interfacial interaction between cavitation and production of radicals.

Declaration of Competing Interest

The authors declare that they have no known competing financial interests or personal relationships that could have appeared to influence the work reported in this paper.

Acknowledgements

The authors would like to express appreciation for the support from Chemistry Department, Universitas Islam Indonesia, through the International Collaboration Program in 2020.

References

[1] S. Khezrianjoo, J. Lee, K.-H. Kim, V. Kumar, Eco-toxicological and kinetic evaluation of TiO2 and ZnO nanophotocatalysts in degradation of organic dye, Catalysts 9 (2019) 871–889.
[2] L. Lin, Y. Chai, B. Zhao, W. Wei, D. He, B. He, et al., Photocatalytic oxidation for degradation of VOCs, Open J. Inorg. Chem. 3 (2013) 14–25, https://doi.org/10.4236/ojic.2013.31003.
[3] H.S. Devi, M.A. Boda, M.A. Shah, S. Parveen, Green Synthesis of Iron Oxide Nanoparticles using Platanus orientalis Leaf Extract for Antifungal Activity, (2019), pp. 38–45.
[4] L. Liu, X. Zhang, L. Yang, L. Ren, D. Wang, J. Ye, Metal nanoparticles induced photocatalysis, Sci. Rev. 4 (2017) 761–780, https://doi.org/10.1093/nsr/nwx019.
[5] S. Bagheri, A. Termehyousefi, T.O. Do, Photocatalytic pathway toward degradation of environmental pharmaceutical pollutants: structure, kinetics and mechanism approach, Catal. Sci. Technol. 7 (2017) 4548–4569, https://doi.org/10.1039/c7cy00468k.
[6] L. Sr, S. Taherian, M.H. Entezari, N. Ghows, Ultrasonics Sonochemistry Sono-Catalytic Degradation and Fast Mineralization of P-Chlorophenol Vol. 20 (2013), pp. 1419–1427.
[7] N.H. Ince, Ultrasound-assisted advanced oxidation processes for water decontamination, Ultrason. Sonochem. 40 (2018) 97–103, https://doi.org/10.1016/j.ultsonch.2017.04.009.
[8] N. Ghows, M.H. Entezari, Kinetic investigation on sono-degradation of Reactive Black 5 with core-shell nanocrystal, Ultrason. Sonochem. 20 (2013) 386–394, https://doi.org/10.1016/j.ultsonch.2012.06.013.
[9] K. Zhang, F.J. Zhang, M.L. Chen, W.C. Oh, Comparison of catalytic activities for photocatalytic and sonocatalytic degradation of methylene blue in present of anatase TiO2-CNT catalysts, Ultrason. Sonochem. 18 (2011) 765–772, https://doi.org/10.1016/j.ultsonch.2010.11.008.
[10] J. Wang, Y. Lv, L. Zhang, B. Liu, R. Jiang, G. Han, et al., Sonocatalytic degradation of organic dyes and comparison of catalytic activities of CeO2/TiO2, SnO2/TiO2 and ZrO2/TiO2 composites under ultrasonic irradiation, Ultrason. Sonochem. 17 (2010) 642–648, https://doi.org/10.1016/j.ultsonch.2009.12.016.
[11] M. Ashokkumar, F. Cavalieri, F. Chemat, K. Okitsu, A. Sambandam, K. Yasui, et al., Handbook of ultrasonics and sonochemistry, in: Ashok kumar (Ed.), Handbook of Ultrasonics and Sonochemistry, 2016, pp. 1–1487, , https://doi.org/10.1007/978-981-287-278-4.
[12] K. Prakash, P. Senthil Kumar, S. Pandiaraj, K. Saravanakumar, S. Karuthapandian, Controllable synthesis of SnO2 photocatalyst with superior photocatalytic activity for the degradation of methylene blue dye solution, J. Exp. Nanosci. 11 (2016) 1138–1155, https://doi.org/10.1080/17458080.2016.1188222.
[13] V. Paramarta, A. Taufik, L. Munisa, R. Saleh, Sono-and photocatalytic activities of SnO2 nanoparticles for degradation of cationic and anionic dyes, AIP Conf. Proc. 1788 (2017) 1–8, https://doi.org/10.1063/1.4968378.
[14] S. Zaman, K. Zhang, A. Karim, J. Xin, T. Sun, J.R. Gong, Sonocatalytic degradation of organic pollutant by SnO 2 /MWCNT nanocomposite, Diam. Relat. Mater. 76 (2017) 177–183, https://doi.org/10.1016/j.diamond.2017.05.009.
[15] M. Honarmand, M. Golmohammadi, A. Naeimi, Green synthesis of SnO2-bentonite nanocomposites for the efficient photodegradation of methylene blue and eriochrome black-T, Mater. Chem. Phys. 241 (2020) 122416, https://doi.org/10.1016/j.matchemphys.2019.122416.
[16] A. Hassani, A. Khataee, S. Karaca, C. Karaca, P. Gholami, Sonocatalytic degradation of ciprofloxacin using synthesized TiO2 nanoparticles on montmorillonite, Ultrason. Sonochem. 35 (2017) 251–262, https://doi.org/10.1016/j.ultsonch.2016.09.027.
[17] H.B. Hadjltaief, A. Omri, M. Ben Zina, P. Da, M.E. Galvez, H.B. Hadjltaief, et al., Titanium dioxide supported on different porous materials as photocatalyst for the degradation of methyl green in wastewaters to cite this version: HAL Id : hal-01255395 titanium dioxide supported on different porous materials as photocatalyst for the deg, Advances in Materials Science and Engineering, (2016), pp. 0–11.
[18] A.T. Babu, R. Antony, Clay semiconductor hetero-system of SnO2/bentonite nanocomposites for catalytic degradation of toxic organic wastes, Appl. Clay Sci. 183 (2019) 105312, , https://doi.org/10.1016/j.clay.2019.105312.
[19] R. Bargougui, K. Omri, A. Mhemdi, S. Ammar, Synthesis and characterization of SnO2 nanoparticles: effect of hydrolysis rate on the optical properties, Adv. Mater. Lett. 6 (2015) 816–819, https://doi.org/10.5185/amlett.2015.5844.
[20] J.K. Kwak, K.H. Park, D.Y. Yun, D.U. Lee, T.W. Kim, D.I. Son, et al., Microstrucural and optical properties of SnO2 nanoparticles formed by using a solvothermal synthesis method, J. Korean Phys. Soc. 57 (2010) 1803–1806, https://doi.org/10.3938/jkps.57.1803.
[21] B. Singh, K. Singh, M. Kumar, S. Thakur, A. Kumar, Insights of preferred growth, elemental and morphological properties of BN/SnO2 composite for photocatalytic applications towards organic pollutants, Chem. Phys. 531 (2020) 110659, https://doi.org/10.1016/j.chemphys.2019.110659.
[22] O. Aguilar, C. Ángeles, C.O. Castillo, C. Martínez, R. Rodríguez, R.S. Ruiz, et al., On the ultrasonic degradation of Rhodamine B in water: kinetics and operational conditions effect, Environ. Technol. (United Kingdom) 35 (2014) 1183–1189, https://doi.org/10.1080/09593330.2013.864711.
[23] M.A. Behnajady, N. Modirshahla, S.B. Tabrizi, S. Molanee, Ultrasonic degradation of Rhodamine B in aqueous solution: influence of operational parameters, J. Hazard. Mater. 152 (2008) 381–386, https://doi.org/10.1016/j.jhazmat.2007.07.019.
[24] S.D. Khairnar, V.S. Shrivastava, Facile synthesis of nickel oxide nanoparticles for the degradation of Methylene blue and Rhodamine B dye: a comparative study, J. Taibah Univ. Sci. 13 (2019) 1108–1118, https://doi.org/10.1080/16583655.2019.1686248.
[25] Y.L. Pang, A.Z. Abdullah, S. Bhatia, Optimization of sonocatalytic degradation of Rhodamine B in aqueous solution in the presence of TiO2 nanotubes using response surface methodology, Chem. Eng. J. 166 (2011) 873–880, https://doi.org/10.1016/j.cej.2010.11.059.
[26] S.P. Patil, B. Bethi, G.H. Sonawane, V.S. Shrivastava, S. Sonawane, Efficient adsorption and photocatalytic degradation of Rhodamine B dye over Bi2O3-bentonite nanocomposites: a kinetic study, J. Ind. Eng. Chem. 34 (2016) 356–363, https://doi.org/10.1016/j.jiec.2015.12.002.

[27] S. Rasalingam, R. Peng, R.T. Koodali, An insight into the adsorption and photocatalytic degradation of rhodamine B in periodic mesoporous materials, Appl. Catal. B 174–175 (2015) 49–59, https://doi.org/10.1016/j.apcatb.2015.02.040.
[28] Z.H. Diao, J.J. Liu, Y.X. Hu, L.J. Kong, D. Jiang, X.R. Xu, Comparative study of Rhodamine B degradation by the systems pyrite/H2O2 and pyrite/persulfate: reactivity, stability, products and mechanism, Sep. Purif. Technol. 184 (2017) 374–383, https://doi.org/10.1016/j.seppur.2017.05.016.
[29] K. Okitsu, B. Nanzai, K. Kawasaki, N. Takenaka, H. Bandow, Sonochemical decomposition of organic acids in aqueous solution: understanding of molecular behavior during cavitation by the analysis of a heterogeneous reaction kinetics model, Ultrason. Sonochem. 16 (2009) 155–162, https://doi.org/10.1016/j.ultsonch.2008.06.006.
[30] S.K. Tang, T.T. Teng, A.F.M. Alkarkhi, Z. Li, Sonocatalytic degradation of rhodamine B in aqueous solution in the presence of Tio2 coated activated carbon, Apcbee Procedia 1 (2012) 110–115, https://doi.org/10.1016/j.apcbee.2012.03.019.
[31] L. Song, Y. Li, S. Zhang, Sonocatalytic degradation of rhodamine B in presence of CdS, Environ. Sci. Pollut. Res. - Int. 25 (2018) 10714–10719, https://doi.org/10.1007/s11356-018-1369-8.
[32] M. Zhou, H. Yang, T. Xian, R.S. Li, H.M. Zhang, X.X. Wang, Sonocatalytic degradation of RhB over LuFeO3 particles under ultrasonic irradiation, J. Hazard. Mater. 289 (2015) 149–157, https://doi.org/10.1016/j.jhazmat.2015.02.054.
[33] L. Nirumand, S. Farhadi, A. Zabardasti, A. Khataee, Synthesis and sonocatalytic performance of a ternary magnetic MIL-101(Cr)/RGO/ZnFe2O4 nanocomposite for degradation of dye pollutants, Ultrason. Sonochem. 42 (2018) 647–658, https://doi.org/10.1016/j.ultsonch.2017.12.033.
[34] C. Lops, A. Ancona, K. Di Cesare, B. Dumontel, N. Garino, G. Canavese, et al., Sonophotocatalytic degradation mechanisms of Rhodamine B dye via radicals generation by micro- and nano-particles of ZnO, Appl. Catal. B 243 (2019) 629–640, https://doi.org/10.1016/j.apcatb.2018.10.078.
[35] J. Kim, B. Park, Y. Son, J. Khim, Peat moss-derived biochar for sonocatalytic applications, Ultrason. Sonochem. 42 (2018) 26–30, https://doi.org/10.1016/j.ultsonch.2017.11.005.
[36] X. Chen, J. Dai, G. Shi, L. Li, G. Wang, H. Yang, Sonocatalytic degradation of Rhodamine B catalyzed by β-Bi2O3 particles under ultrasonic irradiation, Ultrason. Sonochem. 29 (2016) 172–177, https://doi.org/10.1016/j.ultsonch.2015.08.010.